Plasmonic Effect on the Magneto-Optical Property of Monolayer WS$_2$ Studied by Polarized-Raman Spectroscopy

Wuguo Liu [1], Zhongtao Lin [1], Shibing Tian [1], Yuan Huang [1], Huaqing Xue [2], Ke Zhu [1], Changzhi Gu [1,3], Yang Yang [1,*] and Junjie Li [1,3,4,*]

[1] Beijing National Laboratory for Condensed Matter Physics, Institute of Physics, Chinese Academy of Sciences, P.O. Box 603, Beijing 100190, China; wgliu@iphy.ac.cn (W.L.); ztlin@iphy.ac.cn (Z.L.); tianshibing@iphy.ac.cn (S.T.); yhuang01@iphy.ac.cn (Y.H.); zhuke@iphy.ac.cn (K.Z.); czgu@iphy.ac.cn (C.G.)

[2] Research Center of New Energy, Research Institute of Petroleum Exploration & Development, PetroChina, No. 20 Xueyuan Rd., Beijing 100083, China; hqxue@petrochina.com.cn

[3] School of Physical Sciences, University of Chinese Academy of Sciences, Beijing 100049, China

[4] Songshan Lake Materials Laboratory, Dongguan 523808, China

* Correspondence: yang.yang@iphy.ac.cn (Y.Y.); jjli@iphy.ac.cn (J.L.)

Abstract: In recent years, the magneto-optical properties of two-dimensional transition metal disulfides have attracted more and more attention due to their further device applications in spintronics and valleytronics. However, to our knowledge, the plasmonic effect on the magneto-optical properties of WS$_2$ has not been studied. In this work, monolayer WS$_2$ transferred on SiO$_2$/Si substrate and Au film were investigated respectively using polarized-Raman spectroscopy at 4 K under different magnetic fields. Prominent magnetic field–induced variations in the Raman intensities of WS$_2$ samples were observed, which also exhibited significant differences in the spectral evolution versus magnetic field. The resonance magnetic field was 5 T and 5.5 T for the WS$_2$ on SiO$_2$/Si substrate and Au film, respectively. Remarkably, the magneto-optical Raman intensities of A'_1 and 2LA(M) modes for WS$_2$ on Au film were reduced to approximately 60% compared with that of WS$_2$ on SiO$_2$/Si. These results suggest that the plasmonic effect–induced charge transfer plays an important role in the magneto-optical Raman effect of WS$_2$.

Keywords: WS$_2$; Raman; magneto-optical effect; substrate

1. Introduction

Two-dimensional (2D) transition metal disulfides (TMDs), which are composed of strong bonding layers with weak Van der Waals force interlayer attraction and can be stripped into separate atomic layers under certain conditions, have attracted extensive attention in the past 10 years because they exhibit extraordinary physical properties and extensive prospective applications in devices [1–3]. WS$_2$ is a typical 2D TMD, which consists of an S-W-S atomic interlayer. The transition from indirect band gap to direct band gap occurs when the thickness of WS$_2$ decreases to monolayer [4]. Monolayer WS$_2$ has a direct band gap with a theoretical value of ~2.1 eV [5], slightly larger than that of monolayer MoS$_2$. The direct bandgap for monolayer WS$_2$ opens up opportunities for the applications in electronic and optoelectronic devices, such as light-emitting diodes, photodetectors and photoelectric sensors [6,7]. The band structure tunability with strain also meet the needs of field effect transistors (FET) [8,9] and hydrogen evolution [10]. Moreover, WS$_2$ has been considered as a natural candidate for valley research because of the unique symmetry and strong spin-orbit coupling [11].

In recent years, due to the potential device applications in spintronics and valleytronics, increasing research on the magneto-optical properties of 2D TMDs, such as valley Zeeman splitting [12,13], valley-and spin-polarized Landau levels [14], magnetic-field modulated valley polarization and valley coherence [15–17], has been carried out. Optical

spectroscopic methods, such as circular polarized photoluminescence (PL) and magnetic circular dichroism (MCD) have been employed to study the magneto-optical properties of 2D TMDs [18–21]. Applying a magnetic field up to 7 T, a splitting for the PL peaks was observed in WS_2 [19]. Raman spectroscopy has been demonstrated to be a feasible tool to investigate the magneto-optical effect in 2D TMDs [22–24]. Ji et al. observed a giant magneto-optical Raman effect in MoS_2, which was closely related to the symmetry breaking induced by the electron motions modulated by the external magnetic field [22]. In a recent work, reduction of the magneto-optical Raman intensity of MoS_2 was attributed to the lattice defects–induced scattering of electron motion [25]. WS_2 grown on sapphire has been investigated using the magneto-Raman technique at 77 K [24].

It has been demonstrated that localized surface plasmonic resonance (LSPR) occurring on noble metal nanostructures–induced charge transfer from nanostructures to TMDs can prominently enhance the optoelectronic properties of TMDs. The effective hole mobility, up to ~100 (cm^2/Vs,) and high on/off current ratio of >10^6 were observed on the Au decorated WSe_2 [26]. Butun et al. reported a fourfold enhancement in the absorption of a WS_2 film after being hybridized with Ag nanodiscs [27]. The enhanced Raman and PL emission were observed on the hybrids of WS_2 and Au nanoparticles (NPs), which were attributed to the increased internal quantum efficiency and decreased activation energy due to coupling with Au NPs [28]. Thus, the plasmonic effect is predicted to have influence on the magneto-optical properties of WS_2. However, to our knowledge, study of the plasmonic effect on the magneto-optical Raman property of WS_2 has not been reported.

In this work, polarized-Raman spectroscopy was performed on monolayer WS_2 on SiO_2/Si and Au film, respectively, in order to get a clear overview of the plasmonic effect on the magneto-optical property of monolayer WS_2. Dramatic magnetic field–induced modifications of the intensities of Raman modes were observed in WS_2 on different substrates. Moreover, the magneto-optical Raman intensity for WS_2 on Au film was much lower than that for the WS_2 on SiO_2/Si, demonstrating that the charge transfer induced by the surface plasmon that occurs on Au film can offer a significant impact on the magneto-optical Raman effect of monolayer WS_2. Our results provide useful information for understanding the magneto-optical properties of TMDs and the fabrication of TMD-related magneto-optical devices.

2. Materials and Methods

Single-crystalline monolayer WS_2 was prepared using a modified mechanical exfoliation method for bulk crystal and drily transferred onto a 280 nm SiO_2/Si substrate and Au film, respectively. The 10 nm thick Au film was deposited on a 30 nm SiO_2/Si substrate using the magnetron sputtering technique. The number of layers was further confirmed by ultralow frequency (ULF) Raman spectroscopy [29]. Figure 1a shows a white-light micrograph of a mechanical exfoliated WS_2 sample with the thickness overlaid. Large area 1L WS_2 was successfully obtained on a SiO_2/Si substrate. The optical image for monolayer WS_2/Au is similar. Figure 1b presents the magnified scanning electron micrograph (SEM) image of WS_2/Au heterostructure, in which the gray-colored zone indicates the WS_2 transferred. It can be seen clearly that the Au film in fact is composed of aggregated nanoparticles rather a continuous film. The size of nanoparticles (NPs) ranges from 5 to 30 nm. It has been demonstrated that NPs have a higher plasmonic modulation effect than the flat film due to the localized surface plasmon resonance (LSPR) that occurs on NPs. Low-temperature magneto-Raman measurements were performed in a cryostat (attocube AttoDRY 1100) with a custom-designed Raman micro-spectroscopy system. The temperature was fixed at 4 K, while the direction of magnetic field was normal to the sample surface (so-called Faraday geometry) and varied from 0 to 9 T. A linearly polarized 532 nm laser was used as the excitation source, and the power on the sample surface was approximately 2 mW. A low temperature compatible objective (NA = 0.8) was used to focus the laser and collect the Raman signal. The Raman spectra were collected in the parallel-polarized (VV) and crossed-polarized (VH) configurations, as presented

in Figure 1c. In VV configuration, the polarizations of scattered and incident light were parallel to each other, while the polarization of scattered light was perpendicular to that of incident light in VH configuration.
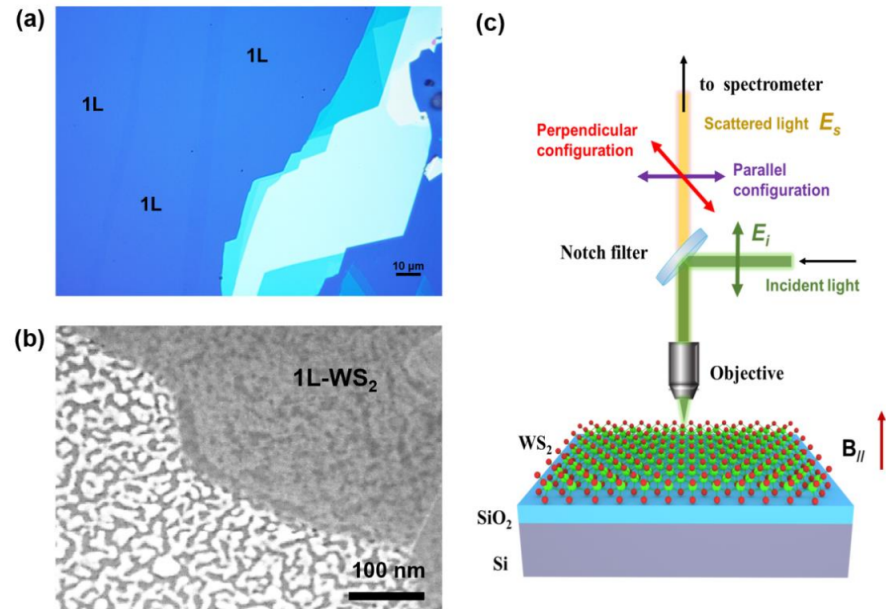

Figure 1. (**a**) Optical image for WS_2 on SiO_2/Si substrate. (**b**) Magnified SEM image of WS_2 on Au film. (**c**) Schematic illustration for the polarized-Raman setup under magnetic field.

3. Results and Discussion

Figure 2 presents the zero-field polarized-Raman spectra of the monolayer WS_2 on SiO_2/Si and Au film, respectively. The Raman spectra of WS_2/SiO_2 exhibit obvious dependence on polarization configurations, as shown in Figure 2a. The line shape of the Raman spectra of the VV spectrum of WS_2/SiO_2 resumes that of monolayer WS_2 in previous literature [11,30]. When the polarization configuration changes from VV to VH, the overall intensity of the spectrum is significantly weakened. After fitting with Lorentzians, five peaks are identified in the range of 250–450 cm^{-1} for the Raman spectra of WS_2/SiO_2, which is consistent with previous literature [31]. Among them, three peaks are worthy of special attention: the second-order resonant peaks involving longitudinal acoustic mode 2LA(M); the in-plane E' vibration mode of two S atoms in the plane in reverse motion with W atom; the out-of-plane A'_1 vibration mode of two S atoms moving backward out of plane [24,32]. At VV configuration, E' mode is just a shoulder peak on the right side of 2LA(M) mode in the Raman spectra of WS_2/SiO_2. And the peak intensities of 2LA(M) and A'_1 are much higher than that of E' mode. In contrast, the intensities of the 2LA(M) and A'_1 modes are obviously weaker relative to E' under VH configuration. The E' mode emerges as an isolated peak, whereas the 2LA(M) mode shrinks significantly. The polarization dependence for the Raman spectra of WS_2/SiO_2 follows the Raman selection rules (RSRs) for WS_2 [24,33].

On the other hand, the Raman spectra of WS_2/Au exhibit prominent different polarization dependent behaviors, as shown in Figure 2b. In sharp contrast to the Raman spectra of WS_2/SiO_2, the spectra lineshapes of WS_2/Au exhibit obvious distinctions. The intensity of 2LA(M) and A'_1 modes are enhanced prominently and become comparable to that of E' mode. Especially in the VH configuration, the intensity of 2LA(M) is still hardening. The Raman spectra in Figure 2b clearly evidence the breaking of RSRs on WS_2/Au, which could be associated with the strong coupling between the plasmon and phonons in WS_2 [34]. As it is well known, the localized electromagnetic (EM) field at close vicinity of the Au NPs can be enhanced due to the LSPR effect under an excitation [35]. The intensity enhancement of the Raman modes for WS_2/Au is attributed to the surface enhanced Raman scattering

(SERS) process as a result of the enhanced EM field [28]. In addition to the SERS process, other physical mechanisms cannot be excluded from the distinct polarized-Raman spectra of WS$_2$/Au. The strain induced by Au NPs underneath also contributes to the intensity enhancement of 2LA(M) mode [36,37].
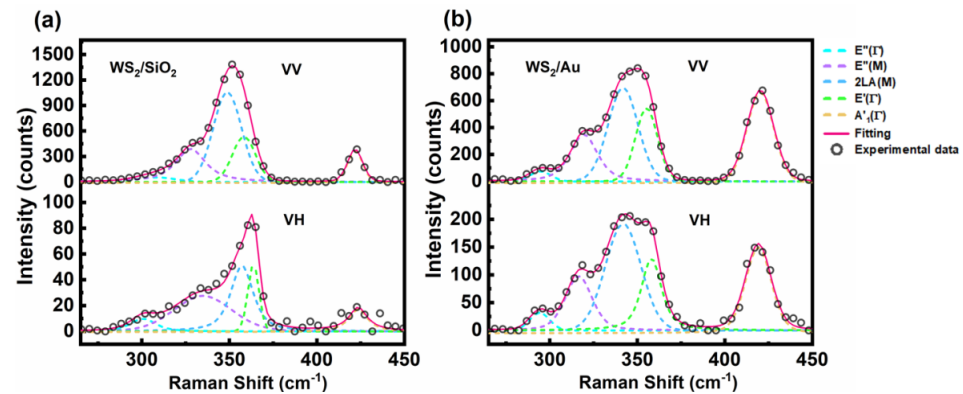

Figure 2. Polarized–Raman spectra of (**a**) WS$_2$/SiO$_2$ and (**b**) WS$_2$/Au collected without magnetic field. Black circles represent the experimental results, the dashed lines are fitting results for each Raman mode, and the red line is the sum of the fitting results.

It has been demonstrated that the A$_1$-symmetry mode is very sensitive to the doping effect [38,39]. For the hybrids composed of TMDs and noble metal NPs, the "hot carriers" are generated and transfer from NPs to WS$_2$ flake under the light illumination [40,41]. Employing ultrafast transient absorption spectroscopy with pumping photon energy below the indirect bandgap of the rippled MoS$_2$ quadrilayer, Camellini et al. directly demonstrated a plasmon-induced charge transfer between Au and MoS$_2$ [42]. As reported by Bhattacharya and coauthors, the Au NPs acted as dopants to WS$_2$ in the plasmonic hybrid nanostructures [28]. The broadening and enhancement of A_1' mode observed in this work is closed related with the electronic doping effect from Au film.

According to the definite lattice orientation for the single crystalline monolayer of WS$_2$, its out-of-plane A_1' and in-plane E' lattice vibrations are aligned with the vertical and horizontal EM fields [43]. The vibrations for LA mode are parallel to the direction of propagation [44,45]. The Raman intensity of E' mode is solely determined by the in-plane horizontal EM fields, whereas the Raman intensities of 2LA(M) and A_1' mode are contributed mainly by the vertical out-of-plane EM field. The prominent enhanced intensities of 2LA(M) and A_1' modes shown in Figure 2b demonstrate that the local EM field in the vertical direction is dominant on the Au NPs prepared in this work. To further study the LSPR effect on the polarized-Raman spectra of TMDs, nanostructures with enhanced EM field along specialized directions, such as dimer or nanogap, should be utilized in the future.

The differences between the Raman spectra for WS$_2$/SiO$_2$ and WS$_2$/Au are closely related to the plasmon-phonon coupling effect. To study the plasmon effect on the magneto-optical property of WS$_2$, the polarized-Raman spectra of WS$_2$/SiO$_2$ and WS$_2$/Au were collected at different magnetic fields. In Figure 3, the spectra were normalized using the intensity of the Raman peak of Si substrate in order to see the intensity evolution of Raman modes of WS$_2$. As displayed in Figure 3a, in VV configuration, the intensity of the Raman spectra decreases with increasing field, reaches the lowest value at approximately 6 T, then recovers with continuously increasing field. Remarkably, the intensity of 2LA(M) and A_1' modes decrease much faster than that of E' mode. The VV spectrum at 6T resembles the features of the VH spectra at 0 T, in which the E' mode becomes an isolated peak. In sharp contrast, the Raman intensity displays an anticorrelated evolution in VH configuration. As shown in Figure 3b, the spectral intensity grows with increasing field up to 6 T, and then recedes with continuously increased field. In particular, the intensity of 2LA(M) and A_1' modes enhances more quickly than that of E' mode. Of note, the VH spectra at 6 T resemble

the features of the VV spectra at 0 T. Overall, one can see that the magnetic field–induced variations for the polarized-Raman spectra of WS_2/SiO_2 exhibit strong similarities with previous reporting [24]. Similar magnetic field modulation behaviors of the polarized-Raman intensity were also reported in MoS_2 [22,25]. The magnetic field–induced electron motion plays a key role in the Raman scattering process. Ji and coauthors proposed a semi-classic scenario to illustrate the magneto-Raman effect in MoS_2 [22]. Under the magnetic field in normal direction to the sample plane, the in-plane electron motion generates a transverse component due to the Lorentz force, leading to a transfer of Raman intensity between the crossed polarization configurations. The elements of Raman tensor, which are normally the electronic susceptibilities with respect to lattice normal coordinates, can be expressed as a function of external field. Therefore, the expression of the measured Raman intensity can be associated with the magnitude of magnetic field and direction of light polarization.
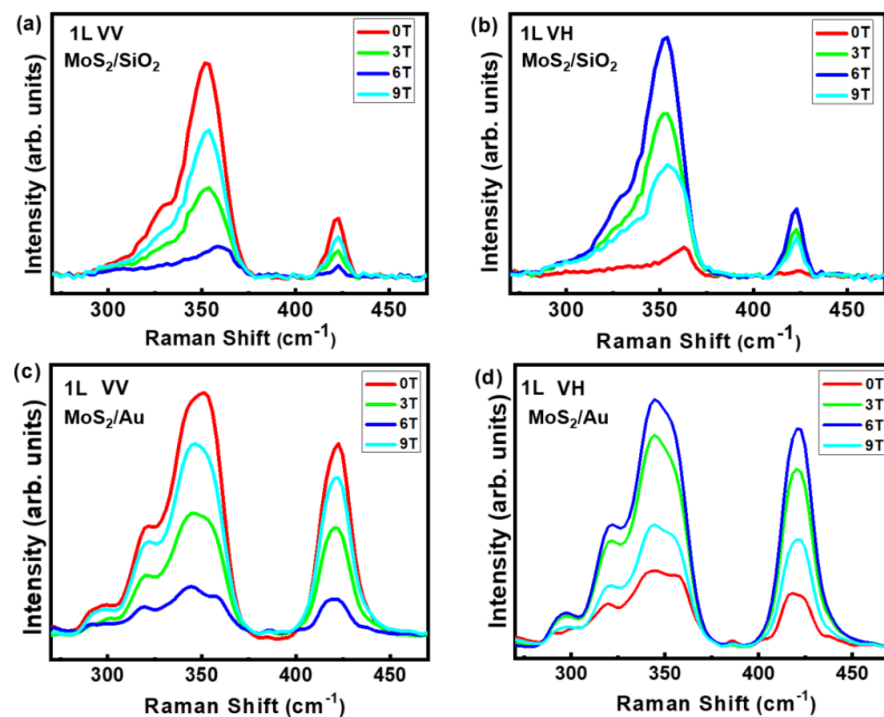

Figure 3. Polarized–Raman spectra of (**a**,**b**) WS_2/SiO_2 and (**c**,**d**) WS_2/Au collected at different magnetic fields.

Magnetic field–induced modulations were also observed on the Raman spectra of WS_2/Au, as shown in Figure 3c,d, which also exhibited obvious intensity fluctuation with increasing field. However, the field-induced variations for WS_2/Au significantly differ from that for WS_2/SiO_2. One can see that both 2LA(M) and E' modes vary significantly with increasing magnetic field in VV configuration. At 6 T, 2LA(M) mode is still clearly identified, and A_1' mode is still greatly residual under VV configuration. The VV spectra at 6 T resembles the line shape of the VH spectra at 0 T.

The magnetic field–dependent Raman spectra for WS_2/SiO_2 and WS_2/Au were de-convoluted using the Lorentz function, in order to get a clear view of the magnetic field dependence of peak intensity of WS_2 on different substrates. As presented in Figure 4a–c, the intensities of 2LA(M), A_1' and E' modes for WS_2/SiO_2 exhibit similar magnetic field dependences. The peak intensities vary oppositely in VV and VH polarization configurations. The maximum intensity in VH configuration and the minimum intensity in VV configuration take place at around 5 T. For simplicity, the magnetic field for the extreme point of intensity is defined as the resonance magnetic field. The similar magnetic field–induced intensity modulations are also observed on WS_2/Au, as displayed in Figure 4d–f.

The resonance magnetic field for WS$_2$/Au is 5.5 T, which is a little higher than that for WS$_2$/SiO$_2$. Noticeable, the intensity amplitudes of 2LA(M), E' and A_1' modes for WS$_2$/Au are very close in VH configuration, which are different from those for WS$_2$/SiO$_2$. The reason for the striking difference between these two WS$_2$ samples is discussed below.
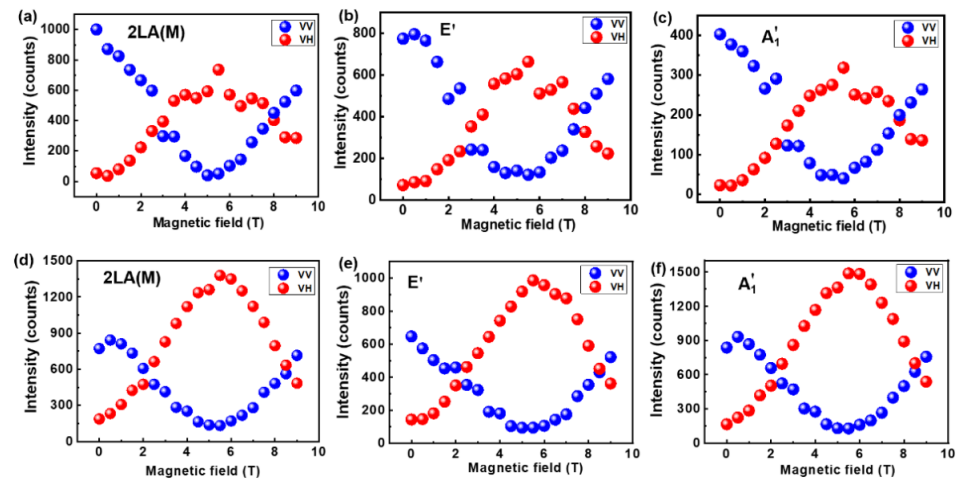

Figure 4. Magnetic field–induced modulation of the Raman intensity in different polarization configurations. (**a–c**) Magnetic field–dependent polarized-Raman intensity of 2LA(M), E' and A_1' modes for WS$_2$/SiO$_2$, respectively. (**d–f**) Magnetic field–dependent polarized-Raman intensity of 2LA(M), E' and A_1' modes for WS$_2$/Au, respectively.

To quantify the effects of magnetic fields on Raman intensity, the magneto-Raman intensity of monolayer WS$_2$ on two different substrates was calculated according to previous literature [24,25], as follows:

$$\text{Magneto-Raman intensity} = \frac{I(B) - I(0)}{I(0)} \times 100\% \tag{1}$$

where $I(B)$ is the Raman intensity obtained under different magnetic fields. As presented in Figure 5a, the magneto-Raman intensity of the 2LA(M), E' and A_1' modes for WS$_2$/SiO$_2$ exhibit a similar variation with increasing magnetic field, which are negative under VV configuration and reach the lowest value at around 5 T. In contrast, the VH polarization configuration witnesses the largest magneto-Raman intensity at 5 T. The VH magneto-Raman intensity of A_1' is higher than that of 2LA(M) and E'. Moreover, the lowest VV magneto-Raman intensity is nearly −100%, whereas the magneto-Raman intensity for the 2LA(M) and A_1' modes boosts to 1300% under VH polarization configuration.

On the other hand, the magneto-Raman intensity for WS$_2$/Au exhibits similar variations as that of WS$_2$/SiO$_2$, as shown in Figure 5c,d. In the VV configuration, the VV magneto-Raman intensity for WS$_2$/Au varies in the range from 20% to −90%, while the highest magneto-Raman intensity is just 800% in the VH configuration. It is worthy to note that the magneto-Raman intensity of A_1' mode for WS$_2$/Au is much lower than that for WS$_2$/SiO$_2$. The magneto-Raman intensities of A_1' and 2LA(M) modes for WS$_2$/Au were reduced to ~60% of that for WS$_2$/SiO$_2$. This difference in the amplitude of the magneto-Raman intensity between WS$_2$/SiO$_2$ and WS$_2$/Au can be attributed to the Au NPs underneath WS$_2$ flake, which breaks the polarization rules for WS$_2$. Due to the light-matter interaction, LSPR takes place at the surface of Au NPs. When plasmonic losses couple to WS$_2$, momentums with different wave vectors are provided by the near-field components in the nanogap between metal NPs [34]. Because the morphologies of Au NPs are irregular, the polarization of electromagnetic wave reflected from Au NPs is randomly distributed. Therefore, the proportions for the Raman signal with different polarizations change as a result of the disturbed polarization of excitation light.
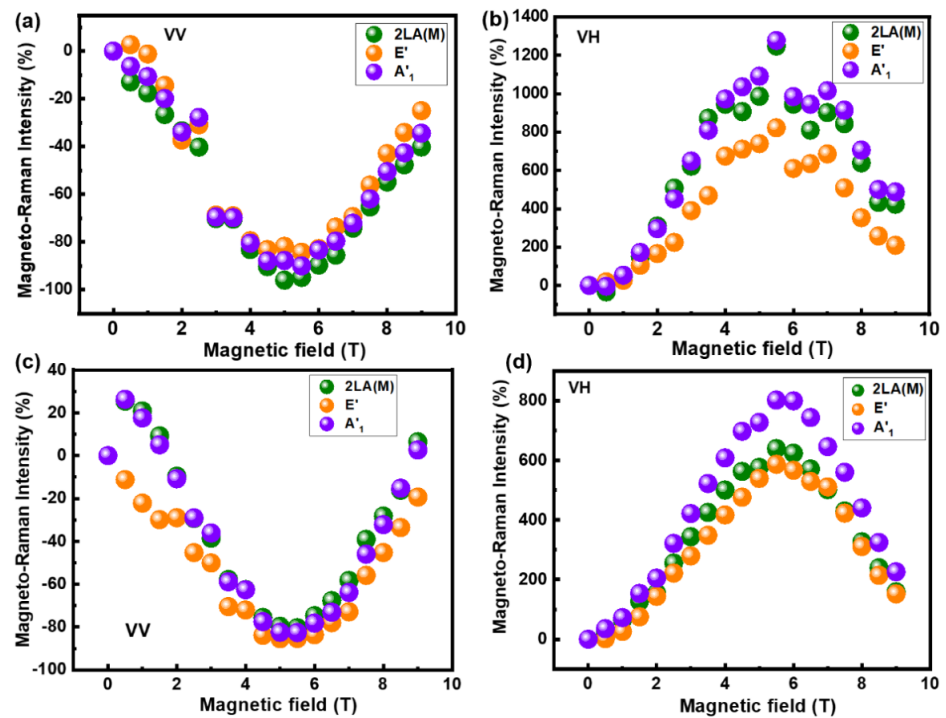
Figure 5. Magneto–Raman intensity for (**a**,**b**) WS_2/SiO_2 and (**c**,**d**) WS_2/Au as a function of magnetic field. Green, orange and purple symbols represent 2LA(M), E' and A'_1 modes, respectively.

Compared with previous literature, the low temperature magneto-optical Raman results obtained in this work exhibit significant difference in resonance magnetic field. Strikingly, the resonance field of monolayer WS_2 in this work (5 T or 5.5 T) is higher than that for the WS_2 grown on sapphire substrate using the CVD method (WS_2/Al_2O_3) at room temperature (4 T) [24]. Based on previous reports, the resonant magnetic field strength is inversely proportional to optical mobility [22]. A smaller optical mobility was predicted for the WS_2 samples in our work according to the results shown in Figures 4 and 5. Normally, the mobility of mechanically exfoliated (ME) WS_2 is higher than that of CVD WS_2 [46]. In addition, as demonstrated on MoS_2, the amplitude of resonance magnetic field at low temperature is smaller than that at high temperature [22,25]. Therefore, the primary origin for the discrepancy in the optical mobility (or resonance magnetic field) between our work and previous reports can be attributed to the different dielectric properties of the substrates used. As the magnetic field effect on Raman process is through the field-modulated motion of electrons [22], the change transfer from the substrate to WS_2 cannot be neglected. The sapphire substrate has a better electronic screening effect than SiO_2. It is assumed that more photon-induced charges can be evolved into the field-modulated Raman process. Moreover, the LSPR induced hot electrons transferred from Au NPs to WS_2, which disturbed the electronic motion under the magnetic fields. Therefore, the resonance magnetic field for WS_2/Au is the highest as compared to WS_2/SiO_2 and WS_2/Al_2O_3. These results suggest that a high-k substrate, such as HfO_2, would be helpful for reducing the resonance magnetic field.

4. Conclusions

To summarize, magneto-Raman spectroscopy has been successfully performed on monolayer WS_2 transferred on SiO_2/Si substrate and Au film, respectively. Dramatic variations of Raman intensity were observed as a function of magnetic field, which can be associated with the symmetry breaking as a result of the electron motion induced by the magnetic field. Strikingly, prominent differences were observed in the magnetic field evolutions for WS_2 on SiO_2/Si substrate and Au film. The magneto-optical Raman intensity for WS_2 on Au film was much lower than that for WS_2 on SiO_2/Si. It is demonstrated

that the plasmonic effect–induced charge transfer plays an important role in the magneto-optical Raman effects of WS_2. Our results provide useful information for understanding the magneto-optical properties of TMDs and further fabricating TMD-based magneto-optical devices.

References

1. Wang, Q.H.; Kalantar-Zadeh, K.; Kis, A.; Coleman, J.N.; Strano, M.S. Electronics and optoelectronics of two-dimensional transition metal dichalcogenides. *Nat. Nanotechnol.* **2012**, *7*, 699–712. [CrossRef]
2. Zhang, X.; Qiao, X.-F.; Shi, W.; Wu, J.-B.; Jiang, D.-S.; Tan, P.-H. Phonon and Raman scattering of two-dimensional transition metal dichalcogenides from monolayer, multilayer to bulk material. *Chem. Soc. Rev.* **2015**, *44*, 2757–2785. [CrossRef] [PubMed]
3. Mueller, T.; Malic, E. Exciton physics and device application of two-dimensional transition metal dichalcogenide semiconductors. *2D Mater. Appl.* **2018**, *2*, 1–12. [CrossRef]
4. Zhao, W.; Ghorannevis, Z.; Chu, L.; Toh, M.; Kloc, C.; Tan, P.-H.; Eda, G. Evolution of electronic structure in atomically thin sheets of WS_2 and WSe_2. *ACS Nano* **2013**, *7*, 791–797. [CrossRef]
5. Kuc, A.; Zibouche, N.; Heine, T. Influence of quantum confinement on the electronic structure of the transition metal sulfide TS_2. *Phys. Rev. B* **2011**, *83*, 245213. [CrossRef]
6. Peimyoo, N.; Yang, W.; Shang, J.; Shen, X.; Wang, Y.; Yu, T. Chemically driven tunable light emission of charged and neutral excitons in monolayer WS_2. *ACS Nano* **2014**, *8*, 11320–11329. [CrossRef]
7. Yin, W.; Bai, X.; Chen, P.; Zhang, X.; Su, L.; Ji, C.; Gao, H.; Song, H.; Yu, W.W. Rational control of size and photoluminescence of WS_2 quantum dots for white light-emitting diodes. *ACS Appl. Mater. Interfaces* **2018**, *10*, 43824–43830. [CrossRef]
8. Georgiou, T.; Jalil, R.; Belle, B.D.; Britnell, L.; Gorbachev, R.V.; Morozov, S.V.; Kim, Y.-J.; Gholinia, A.; Haigh, S.J.; Makarovsky, O. Vertical field-effect transistor based on graphene–WS_2 heterostructures for flexible and transparent electronics. *Nat. Nanotechnol.* **2013**, *8*, 100. [CrossRef]
9. Sik Hwang, W.; Remskar, M.; Yan, R.; Protasenko, V.; Tahy, K.; Doo Chae, S.; Zhao, P.; Konar, A.; Xing, H.; Seabaugh, A. Transistors with chemically synthesized layered semiconductor WS_2 exhibiting 10^5 room temperature modulation and ambipolar behavior. *Appl. Phys. Lett.* **2012**, *101*, 013107. [CrossRef]
10. Voiry, D.; Yamaguchi, H.; Li, J.; Silva, R.; Alves, D.C.; Fujita, T.; Chen, M.; Asefa, T.; Shenoy, V.B.; Eda, G. Enhanced catalytic activity in strained chemically exfoliated WS_2 nanosheets for hydrogen evolution. *Nat. Mater.* **2013**, *12*, 850–855. [CrossRef]
11. Zeng, H.; Liu, G.-B.; Dai, J.; Yan, Y.; Zhu, B.; He, R.; Xie, L.; Xu, S.; Chen, X.; Yao, W. Optical signature of symmetry variations and spin-valley coupling in atomically thin tungsten dichalcogenides. *Sci. Rep.* **2013**, *3*, 1608. [CrossRef]
12. Srivastava, A.; Sidler, M.; Allain, A.V.; Lembke, D.S.; Kis, A.; Imamoğlu, A. Valley Zeeman effect in elementary optical excitations of monolayer WSe_2. *Nat. Phys.* **2015**, *11*, 141–147. [CrossRef]
13. Aivazian, G.; Gong, Z.; Jones, A.M.; Chu, R.-L.; Yan, J.; Mandrus, D.G.; Zhang, C.; Cobden, D.; Yao, W.; Xu, X. Magnetic control of valley pseudospin in monolayer WSe 2. *Nat. Phys.* **2015**, *11*, 148–152. [CrossRef]
14. Wang, Z.; Shan, J.; Mak, K.F. Valley-and spin-polarized Landau levels in monolayer WSe_2. *Nat. Nanotechnol.* **2017**, *12*, 144. [CrossRef]
15. Smoleński, T.; Goryca, M.; Koperski, M.; Faugeras, C.; Kazimierczuk, T.; Bogucki, A.; Nogajewski, K.; Kossacki, P.; Potemski, M. Tuning valley polarization in a WSe_2 monolayer with a tiny magnetic field. *Phys. Rev. X* **2016**, *6*, 021024.
16. Schmidt, R.; Arora, A.; Plechinger, G.; Nagler, P.; del Aguila, A.G.; Ballottin, M.V.; Christianen, P.C.; de Vasconcellos, S.M.; Schüller, C.; Korn, T. Magnetic-field-induced rotation of polarized light emission from monolayer WS_2. *Phys. Rev. Lett.* **2016**, *117*, 077402. [CrossRef] [PubMed]
17. Norden, T.; Zhao, C.; Zhang, P.; Sabirianov, R.; Petrou, A.; Zeng, H. Giant valley splitting in monolayer WS_2 by magnetic proximity effect. *Nat. Commun.* **2019**, *10*, 1–10. [CrossRef] [PubMed]

18. Branny, A.; Wang, G.; Kumar, S.; Robert, C.; Lassagne, B.; Marie, X.; Gerardot, B.D.; Urbaszek, B. Discrete quantum dot like emitters in monolayer $MoSe_2$: Spatial mapping, magneto-optics, and charge tuning. *Appl. Phys. Lett.* **2016**, *108*, 142101. [CrossRef]

19. Kuhnert, J.; Rahimi-Iman, A.; Heimbrodt, W. Magneto photoluminescence measurements of tungsten disulphide monolayers. *J. Phys. Condens. Matter* **2017**, *29*, 08LT02. [CrossRef] [PubMed]

20. Zou, C.; Cong, C.; Shang, J.; Zhao, C.; Eginligil, M.; Wu, L.; Chen, Y.; Zhang, H.; Feng, S.; Zhang, J. Probing magnetic-proximity-effect enlarged valley splitting in monolayer WSe_2 by photoluminescence. *Nano Res.* **2018**, *11*, 6252–6259. [CrossRef]

21. Wu, Y.; Shen, C.; Tan, Q.; Shi, J.; Liu, X.; Wu, Z.; Zhang, J.; Tan, P.; Zheng, H. Valley Zeeman splitting of monolayer MoS_2 probed by low-field magnetic circular dichroism spectroscopy at room temperature. *Appl. Phys. Lett.* **2018**, *112*, 153105. [CrossRef]

22. Ji, J.; Zhang, A.; Fan, J.; Li, Y.; Wang, X.; Zhang, J.; Plummer, E.; Zhang, Q. Giant magneto-optical Raman effect in a layered transition metal compound. *Proc. Natl. Acad. Sci. USA* **2016**, *113*, 2349–2353. [CrossRef]

23. Du, L.; Zhang, Q.; Gong, B.; Liao, M.; Zhu, J.; Yu, H.; He, R.; Liu, K.; Yang, R.; Shi, D. Robust spin-valley polarization in commensurate MoS_2/graphene heterostructures. *Phys. Rev. B* **2018**, *97*, 115445. [CrossRef]

24. Du, L.; Jia, Z.; Zhang, Q.; Zhang, A.; Zhang, T.; He, R.; Yang, R.; Shi, D.; Yao, Y.; Xiang, J. Electronic structure-dependent magneto-optical Raman effect in atomically thin WS_2. *2D Mater.* **2018**, *5*, 035028. [CrossRef]

25. Yang, Y.; Liu, W.; Lin, Z.; Zhu, K.; Tian, S.; Huang, Y.; Gu, C.; Li, J. Micro-Defects in Monolayer MoS_2 Studied by Low-Temperature Magneto-Raman Mapping. *J. Phys. Chem. C* **2020**, *124*, 17418–17422. [CrossRef]

26. Chen, C.-H.; Wu, C.-L.; Pu, J.; Chiu, M.-H.; Kumar, P.; Takenobu, T.; Li, L.-J. Hole mobility enhancement and p-doping in monolayer WSe_2 by gold decoration. *2D Mater.* **2014**, *1*, 034001. [CrossRef]

27. Butun, S.; Palacios, E.; Cain, J.D.; Liu, Z.; Dravid, V.P.; Aydin, K. Quantifying plasmon-enhanced light absorption in monolayer WS_2 films. *ACS Appl. Mater. Interfaces* **2017**, *9*, 15044–15051. [CrossRef]

28. Bhattacharya, T.S.; Mitra, S.; Singha, S.S.; Mondal, P.K.; Singha, A. Tailoring light-matter interaction in WS_2–gold nanoparticles hybrid systems. *Phys. Rev. B* **2019**, *100*, 235438. [CrossRef]

29. Tan, Q.-H.; Sun, Y.-J.; Liu, X.-L.; Zhao, Y.; Xiong, Q.; Tan, P.-H.; Zhang, J. Observation of forbidden phonons, Fano resonance and dark excitons by resonance Raman scattering in few-layer WS_2. *2D Mater.* **2017**, *4*, 031007. [CrossRef]

30. Huang, X.; Gao, Y.; Yang, T.; Ren, W.; Cheng, H.-M.; Lai, T. Quantitative Analysis of Temperature Dependence of Raman shift of monolayer WS_2. *Sci. Rep.* **2016**, *6*, 32236. [CrossRef] [PubMed]

31. Zhang, X.; Tan, Q.-H.; Wu, J.-B.; Shi, W.; Tan, P.-H. Review on the Raman spectroscopy of different types of layered materials. *Nanoscale* **2016**, *8*, 6435–6450. [CrossRef]

32. Zhang, S.; Zhang, N.; Zhao, Y.; Cheng, T.; Li, X.; Feng, R.; Xu, H.; Liu, Z.; Zhang, J.; Tong, L. Spotting the differences in two-dimensional materials–the Raman scattering perspective. *Chem. Soc. Rev.* **2018**, *47*, 3217–3240. [CrossRef] [PubMed]

33. Ribeiro-Soares, J.; Almeida, R.; Barros, E.B.; Araujo, P.T.; Dresselhaus, M.S.; Cançado, L.G.; Jorio, A. Group theory analysis of phonons in two-dimensional transition metal dichalcogenides. *Phys. Rev. B* **2014**, *90*, 115438. [CrossRef]

34. Zhao, W.; Wu, Q.; Hao, Q.; Wang, J.; Li, M.; Zhang, Y.; Bi, K.; Chen, Y.; Ni, Z. Plasmon–phonon coupling in monolayer WS_2. *Appl. Phys. Lett.* **2016**, *108*, 131903. [CrossRef]

35. Reguera, J.; Langer, J.; de Aberasturi, D.J.; Liz-Marzan, L.M. Anisotropic metal nanoparticles for surface enhanced Raman scattering. *Chem. Soc. Rev.* **2017**, *46*, 3866–3885. [CrossRef]

36. Jeong, H.; Oh, H.M.; Gokarna, A.; Kim, H.; Yun, S.J.; Han, G.H.; Jeong, M.S.; Lee, Y.H.; Lerondel, G. Integrated Freestanding Two-dimensional Transition Metal Dichalcogenides. *Adv. Mater.* **2017**, *29*, 1700308. [CrossRef]

37. Khalil, H.M.; Khan, M.F.; Eom, J.; Noh, H. Highly stable and tunable chemical doping of multilayer WS_2 field effect transistor: Reduction in contact resistance. *ACS Appl. Mater. Interfaces* **2015**, *7*, 23589–23596. [CrossRef]

38. Iqbal, M.W.; Shahzad, K.; Akbar, R.; Hussain, G. A review on Raman finger prints of doping and strain effect in TMDCs. *Microelectron. Eng.* **2020**, *219*, 111152. [CrossRef]

39. Mlack, J.T.; Das, P.M.; Danda, G.; Chou, Y.-C.; Naylor, C.H.; Lin, Z.; López, N.P.; Zhang, T.; Terrones, M.; Johnson, A.C. Transfer of monolayer TMD WS_2 and Raman study of substrate effects. *Sci. Rep.* **2017**, *7*, 43037. [CrossRef]

40. Zeng, Y.; Li, X.; Chen, W.; Liao, J.; Lou, J.; Chen, Q. Highly Enhanced Photoluminescence of Monolayer MoS_2 with Self-Assembled Au Nanoparticle Arrays. *Adv. Mater. Interfaces* **2017**, *4*, 1700739. [CrossRef]

41. Kang, Y.; Gong, Y.; Hu, Z.; Li, Z.; Qiu, Z.; Zhu, X.; Ajayan, P.M.; Fang, Z. Plasmonic hot electron enhanced MoS_2 photocatalysis in hydrogen evolution. *Nanoscale* **2015**, *7*, 4482–4488. [CrossRef] [PubMed]

42. Camellini, A.; Mazzanti, A.; Mennucci, C.; Martella, C.; Lamperti, A.; Molle, A.; Buatier de Mongeot, F.; Della Valle, G.; Zavelani-Rossi, M. Evidence of Plasmon Enhanced Charge Transfer in Large-Area Hybrid Au-MoS_2 Metasurface. *Adv. Opt. Mater.* **2020**, *8*, 2000653. [CrossRef]

43. Chen, W.; Zhang, S.P.; Kang, M.; Liu, W.K.; Ou, Z.W.; Li, Y.; Zhang, Y.X.; Guan, Z.Q.; Xu, H.X. Probing the limits of plasmonic enhancement using a two-dimensional atomic crystal probe. *Light Sci. Appl.* **2018**, *7*, 1–11. [CrossRef]

44. Vacher, R.; Boyer, L. Brillouin-scattering: A tool for measurement of elastic and photoelastic constants. *Phys. Rev. B Solid State* **1972**, *6*, 639. [CrossRef]

45. Neighbours, J.R.; Schacher, G.E. Determination of elastic constants from sound-velocity measurements in crystals of general symmetry. *J. Appl. Phys.* **1967**, *38*, 5366. [CrossRef]

46. Reale, F.; Palczynski, P.; Amit, I.; Jones, G.F.; Mehew, J.D.; Bacon, A.; Ni, N.; Sherrell, P.C.; Agnoli, S.; Craciun, M.F. High-mobility and high-optical quality atomically thin WS_2. *Sci. Rep.* **2017**, *7*, 1–10. [CrossRef] [PubMed]